Composite Structures, 132:621–632, 2015

Analytical Solution for Plane Stress/Strain Deformation of Laminates with Matrix Cracks

Ever J. Barbero,[1]
Javier Cabrera Barbero,[2]
and Carlos Navarro Ugena[3]

Abstract

An analytical, closed form solution for $[0_m/90_n/\pm\theta_r]_s$ laminated composites with transverse matrix cracks is presented. The deformation is shown to consist of a homogeneous deformation plus a perturbation near the crack. A methodology is proposed to separate the perturbation from the homogeneous deformation to eliminate ill-conditioning of the eigenvalue/eigenvector problem. While the homogeneous deformation provides a macroscopic measure of damage in terms of reduced stiffness of the laminate, the perturbation solution provides the intralaminar shear near the crack, which is used to calculate the extent of shear lag and the maximum intralaminar shear stress. The equations of elasticity are reduced to one-dimension in a two-step approach, first assuming plane strain (stress) along one of the in-plane dimensions and then introducing approximations through the thickness of the laminate. The intact portion of the laminate is modeled without using a single equivalent laminate. Furthermore, plies are subdivided into multiple sub-plies to increase the accuracy of the representation of intralaminar/interlaminar shear, which is shown to have relevance on the predicted value of maximum interlaminar shear stress and is crucial for the prediction of matrix-crack induced delamination.

Keywords

Matrix damage; Intralaminar damage; Shear lag; Ineffective length; Analytical solution; Laminated plate kinematics.

1 Introduction

Intralaminar matrix cracking is the first mode of damage in polymer-matrix laminated composites subjected to quasi-static, fatigue, and impact load [1]. Matrix cracks are caused by a combination of transverse tensile and in-plane shear strain [2]. Under these conditions, preexisting defects

[1]Professor, West Virginia University, Morgantown, USA. Corresponding author.
[2]Undergraduate student, Universidad Carlos III de Madrid, Madrid, Spain.
[3]Catedrático, Universidad Carlos III de Madrid, Madrid, Spain
The final publication is available at `http://dx.doi.org/10.1016/j.compstruct.2015.06.010`

grow into cracks when the energy release rate exceeds the intralaminar fracture toughness of the lamina [3]. Matrix cracking increases the permeability of the laminate leading to gas/liquid leakage and facilitates access to contaminants that may degrade the fibers. Also, matrix cracking often precedes catastrophic modes of damage such as delamination [4], and fatigue life reduction [1]. Finally, stiffness reduction of cracking laminas leads to stress redistribution to other laminas that may as a result fail in a catastrophic, fiber dominated mode. Therefore, prediction of damage initiation and evolution is an important ingredient of laminate failure prediction [5].

Many attempts have been made to predict initiation and evolution of matrix cracks in laminated, polymer-matrix composites. This work focuses on methods that require the minimum number of material properties to achieve predictions that compare well with available experimental data. Such focus precludes all methods that require adjustable parameters, for example in the form of empirical hardening laws [6,7]. The remaining methods include those based exclusively on fracture mechanics [8–10] and those based on combinations of fracture and strength, for example [11, 12]. Furthermore, our study is limited to linear elastic/damaging materials without interface damage [13] or delaminations [14, 15]. Under these restrictions, solutions are available that are either approximate, e.g., [16, 17] or numerical, e.g., [18–21]. Both approximate and numerical solutions require either experiments or analytical solutions to validate them. Experiments are limited to a few laminate configurations and they are further limited in what can be measured. For example, stiffness reduction of carbon fiber laminates is very difficult to measure. Therefore, analytical solutions are desirable because they can be used as benchmarks, even if they are limited in scope of applicability to say, plane strain or plane stress, and even if they clearly impose restrictions on the type of material behavior, such as say, elastically linear/damaging behavior.

Experimentally, it has been shown that unidirectional loading of $[0_m/90_n]$ cross-ply laminates produces matrix cracking of the 90°-lamina when the load is applied in 0°-direction [16, 22–27]. Some models based on those observations are, for example [22] for $[0/90_n]$ laminates and [28] for $[\pm\theta/90_n]$ laminates.

An analytical, yet approximate solution for laminate stiffness reduction due to matrix cracking in of at most two laminas at different angles is presented in [17] using oblique coordinates mathematics. The 3D equations of elasticity are reduced to 2D by certain approximations, of which the most notable is the assumption of layerwise linear distribution of intralaminar stress. Since the resulting system is 2D, a system of partial differential equations (PDE) must be solved. The solution is approximate because there is no general, closed form solution for PDE's. Based on this solution, a unified damage initiation and evolution criterion was added in [29] to allow prediction of crack density as a function of applied strain. A simpler solution in Cartesian coordinates is possible by specializing such solution for only one damaging lamina [30]. Furthermore, continuum damage mechanics (CDM) allows to extend the solution method to any number of laminas, which may damage simultaneously [30]. Comparison with experimental data is very good [31–33].

The number of approximations made on the aforementioned solutions can be reduced by reducing the dimensionality to 1D. In this way, a 3D problem reduces to a system of ordinary differential equations (ODE) for which a closed, analytical solution can be found. Although this limits the applicability of the solution, important structures can be analyzed this way. Aircraft wings, fuselages, and all types of masts can be treated on a first approximation as high aspect ratio structures that are basically in a state of plane strain along the length and plane stress through the thickness [34]. On the other hand, beams can be assumed to be in a state of plane stress throughout both the width and thickness. In addition, the proposed plane strain (stress) analytical solution can be used as a benchmark for approximate numerical solutions that may be developed in the future.

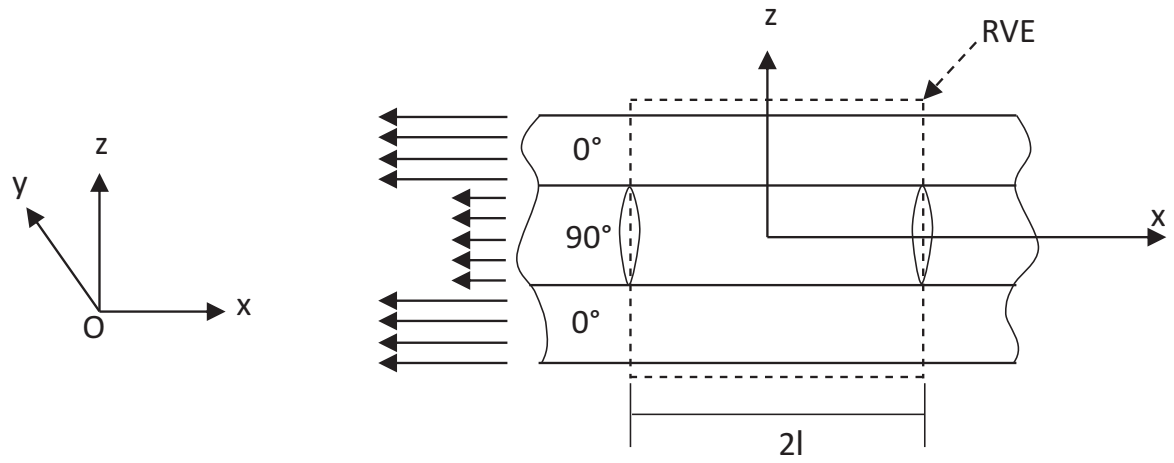

Figure 1: Representative Volume Element (RVE) with dimensions $2\ell \times 1 \times 2h$, where $2h$ is the thickness of the laminate.

2 Approximations

2.1 Fracture mechanics

Consider a thin, symmetric, balanced laminate, with $2N$ laminas, subjected to membrane load N_x only. All laminas are of the same material but oriented with respect to the x-axis in a laminate stacking sequence such as $[0_m/90_n/\pm\theta_r]_S$, where $\theta < 45°$. Experimental evidence [25, 26, 35–37] indicate that in such laminates, the transverse laminas develop cracks as soon as the energy release rate in mode-I fracture G_I exceeds the intralaminar fracture toughness of the material G_{Ic}. Cracks start at defects within the transverse lamina (90_n lamina). Their propagation through the thickness of the lamina is unstable [38, section 7.2.1], reaching the interface suddenly. Upon further increase in applied load N_x or strain ϵ_x^0, the thickness cracks grow again unstably parallel to the fiber direction, as illustrated in Figure 1.

Initially, these long, parallel cracks are not equally spaced but they become so as the crack density increases [39]. It is therefore possible to assume equally spaced cracks, which allows us to identify and use a representative volume element (RVE) to analyze this problem efficiently. The RVE encompasses the thickness of the bottom symmetric part of the laminate, a unit length along the fiber direction of the cracking lamina, and the distance 2ℓ between existing cracks. The crack density in each lamina is defined as

$$\lambda_i = 1/2\ell \tag{1}$$

The analysis assumes that a very small crack density exists in the material, which may be justified as being representative of initial defects. An initial value $\lambda_i = 0.01\, mm^{-1}$ is used in the examples. New cracks are assumed to appear halfway between existing cracks, that is, as far as possible of the shear lag regions near existing cracks. The coordinate system for the RVE has its origin halfway between existing cracks, as shown in Figure 1.

2.2 Plate kinematics

Due to symmetry of geometry, loads, and material properties with respect to the mid-surface of the laminate, only the bottom half of laminate (N laminas) needs to be analyzed. Since the laminate is thin,

I. Lines initially normal to the mid-surface remain incompressible ($\epsilon_z \simeq 0$)

II. The deflection w^0 and the rotations ϕ_x^0, ϕ_y^0, are very small (small deformations and infinitesimal strains)

Assuming the laminate is only subject to membrane loads, there is no transverse deflection of the mid-surface $w^0 = 0$. Further, a state of plane stress is assumed, so

$$\sigma_z^i = 0 \tag{2}$$

$$w^i = w^0 = 0 \tag{3}$$

for all $i = 1 \dots N$ laminas. If the laminate is very long in the $y-$direction (plane strain)

$$\frac{\partial()^i}{\partial y} = 0 \tag{4}$$

Conversely, if the laminate is very narrow in the $y-$direction (plane stress)

$$\sigma_y = 0 \tag{5}$$

as in beam theory. Assuming that the laminate is balanced, such as $[0_m/90_n/\pm\theta_r]$, the in-plane shear stresses cancel out, $\gamma_{xy}^0 = 0$. Furthermore, each pair of angle-ply laminas $[\pm\theta_r]$ is treated as a single lamina with the stiffness equation as follows

$$[Q] = \frac{(Q^\theta + Q^{-\theta})}{2} \tag{6}$$

Therefore,

$$\gamma_{xy}^i = \frac{\partial u^i}{\partial y} + \frac{\partial v^i}{\partial x} = 0 \tag{7}$$

For plane strain, taking into account (4), $v^i = v^i(z)$ is a function of z only. For plane stress, using (5), $v^i = v^i(y, z)$ is a function of y and z only. Assuming that matrix cracks appear only in the transverse laminas (with orientation $\theta = 90$), the domain is symmetric with respect to the x-z plane. Therefore,

$$\gamma_{yz}^i = \frac{\partial w^i}{\partial y} + \frac{\partial v^i}{\partial z} = 0 \tag{8}$$

Taking into account (4–5) for plane strain/stress and (8), the sum of the approximations introduced so far, reduces the problem to 2D, i.e.,

$$\begin{cases} u^i = u^i(x,z) = u_o(x) + u_1^i(x,z) \\ v^i = 0 \text{ (plane strain), or } v^i = v_o(y) \text{ (plane stress)} \\ w^i = 0 \end{cases} \tag{9}$$

and

$$\epsilon_x^i = \frac{\partial u^i}{\partial x} = \frac{\partial u_o(x)}{\partial x} + \frac{\partial u_1^i(x,z)}{\partial x} \tag{10}$$

where $u_o(x)$ is the fundamental homogenous solution and $u_1^i(x,z)$ are perturbations produced by intralaminar cracks.

3 Constitutive equations

Let's denote by subscript k the particular lamina that is, at the moment, subject to cracking, which in this study will be one of the laminas oriented at 90 degrees with respect to the x-axis, taken one at a time. Let's denote with subscript $m \neq k$ all other laminas that are not cracking at the moment, which are N-1 of them. If more than one transverse lamina exist, they will be analyzed one at a time. For a state of plane stress through the thickness of the laminate ($\epsilon_z \approx 0$) we have

$$\begin{Bmatrix} \epsilon_x \\ \epsilon_y \\ \gamma_{xy} = 0 \end{Bmatrix}^i = \begin{bmatrix} \bar{S}_{11} & \bar{S}_{12} & \bar{S}_{16} \\ \bar{S}_{12} & \bar{S}_{22} & \bar{S}_{26} \\ \bar{S}_{16} & \bar{S}_{26} & \bar{S}_{66} \end{bmatrix}^i \begin{Bmatrix} \sigma_x \\ \sigma_y \\ \sigma_{xy} \end{Bmatrix}^i ; \quad \begin{Bmatrix} \gamma_{yz} = 0 \\ \gamma_{xz} \end{Bmatrix}^i = \begin{bmatrix} \bar{S}_{44} & \bar{S}_{45} \\ \bar{S}_{45} & \bar{S}_{55} \end{bmatrix}^i \begin{Bmatrix} \tau_{yz} \\ \tau_{xz} \end{Bmatrix}^i \tag{11}$$

where $\epsilon_y = 0$ and $\sigma_y \neq 0$ for plane strain along y, or $\sigma_y = 0$ and $\epsilon_y \neq 0$ for plane stress along y, for all laminas $i = 1 \dots N$. Note that each balanced pair $\pm\theta$ is treated as a single lamina with the properties of the θ lamina except that $\bar{S}_{16} = \bar{S}_{26} = \bar{S}_{45} = 0$ as a result of (6). Therefore, the problem has symmetry with respect to the x-z plane, and $\tau^i_{yz} = 0$. Using these facts in (11), we get

$$\frac{\partial u^i}{\partial z} = \bar{S}^i_{55}\, \tau^i_{xz} \tag{12}$$

The constitutive equation of lamina i, expressed in lamina coordinate system (c.s. 1,2,3), and taking the average (20) over the ply thickness, is

$$\widehat{\sigma}^i_r = \left[Q^i_{rs}\right] (\widehat{\epsilon}^i_s - \widehat{\alpha}^i_s \Delta T); \quad r, s = 1, 2, 6 \tag{13}$$

where α is the coefficient of thermal expansion (CTE), ΔT is the increment of temperature, and $[Q^i_{rs}]$ is the stiffness matrix of the lamina, possibly reduced due to prior damage, and expressed in the lamina c.s. Once the crack density λ_k in lamina k is known, and the reduced stiffness of the laminate $[Q(\lambda)]$ has been calculated, the reduced stiffness matrix $[Q^k]$ of lamina k can be calculated as

$$[Q^k]\, h^k = [Q(\lambda)]\, h - \sum_{m=1}^{N} (1 - \delta_{mk}) [Q^m]\, h_m \tag{14}$$

where δ is the Kronecker symbol and $h = \sum_{i=1}^{N} h_i$ is the thickness of the symmetric part of the laminate. To aid in computer implementation, the following damage variables are defined

$$D^k_{ij}(\lambda_k) = 1 - Q^k_{ij}/\widetilde{Q}^k_{ij}; \quad i = 1, 2, 6 \; ; \; j = 2, 6 \tag{15}$$

where $\widetilde{Q}^k_{ij}$ is the virgin stiffness matrix of the lamina. In this way, the reduced stiffness of any damaged lamina can be easily calculated as

$$\left[Q^k\right] = \begin{bmatrix} \widetilde{Q}^k_{11} & (1 - D_{12})\widetilde{Q}^k_{12} & 0 \\ (1 - D_{12})\widetilde{Q}^k_{12} & (1 - D_{22})\widetilde{Q}^k_{22} & 0 \\ 0 & 0 & (1 - D_{66})\widetilde{Q}^k_{66} \end{bmatrix} \tag{16}$$

Based on experimental evidence [25,26,35,36] among others, laminas at 0° and groups $\pm\theta < 45°$, denoted by subscript m, are assumed to be free from cracking when loaded with N_x only. Laminas at 90°, denoted by subscript k, are assumed to crack when the energy release rate in fracture mode I, reaches the intralaminar fracture toughness G_{Ic}.

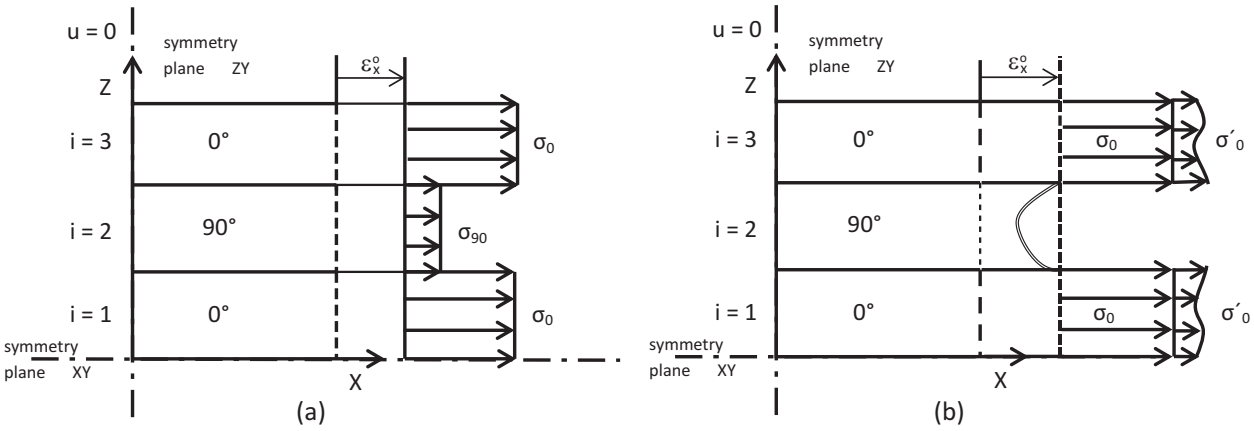

Figure 2: Through-the-thickness distribution of normal stress (a) before and (b) after the crack.

For plane strain along the $y-$direction, (13) becomes

$$\begin{aligned}\widehat{\sigma}_x &= \bar{Q}^i_{11}\widehat{\epsilon}_x - (\widehat{\alpha}^i_x\bar{Q}^i_{11} + \widehat{\alpha}^i_y\bar{Q}^i_{12})\Delta T \\ \widehat{\sigma}_y &= \bar{Q}^i_{12}\widehat{\epsilon}_x - (\widehat{\alpha}^i_x\bar{Q}^i_{12} + \widehat{\alpha}^i_y\bar{Q}^i_{22})\Delta T\end{aligned} \tag{17}$$

where $\bar{Q}^i$ and $\widehat{\alpha}^i$ is the lamina stiffness matrix and coefficient of thermal expansion respectively, transformed to the laminate coordinate system x,y.

For plane stress along the $y-$direction, (13) becomes

$$\begin{aligned}\widehat{\sigma}_x &= E^i_x(\widehat{\epsilon}_x - \widehat{\alpha}^i_x\Delta T) \\ \widehat{\sigma}_y &= 0\end{aligned} \tag{18}$$

where E^i_x is the modulus of elasticity of the $i-$lamina in the laminate coordinate system x,y

$$E^i_x = \bar{Q}^i_{11} - \frac{(\bar{Q}^i_{12})^2}{\bar{Q}^i_{22}} \tag{19}$$

4 Deformation

Applying a uniaxial membrane load N_x or temperature increment ΔT, a thin, symmetric laminate without cracks undergoes uniform deformation $u_o(x) = \epsilon^0 x$ with constant strain ϵ^0. Due to the different stiffness of the laminas, the stress distribution is piecewise constant through the thickness, as show in Figure 2.a. For the undamaged laminate, no interlaminar shear is necessary to satisfy continuity of displacements through the thickness at any position x along the laminate.

If a crack appears in lamina k, the surface of the crack becomes a free edge, unable to support stress. To maintain equilibrium, the stress in the remaining laminas must increase, as depicted in Figure 2.b. In this example, $k = 2$. Lamina $k = 5$ is also cracking due to symmetry but it does not participate directly in the analysis. The resulting stress distribution is unknown and not necessarily piecewise constant but it must remain symmetric because the laminate is symmetric. Even though only half of the laminate is analyzed, all events, such as crack formation, are symmetric. Also the deformation of the crack surface is unknown but it must be symmetric with respect to the centerline of the cracked lamina.

Since the cracked lamina does not carry axial stress but it is still bonded to the adjacent laminas, interlaminar stress τ_{xz} is necessary to satisfy continuity of displacements at the interface between

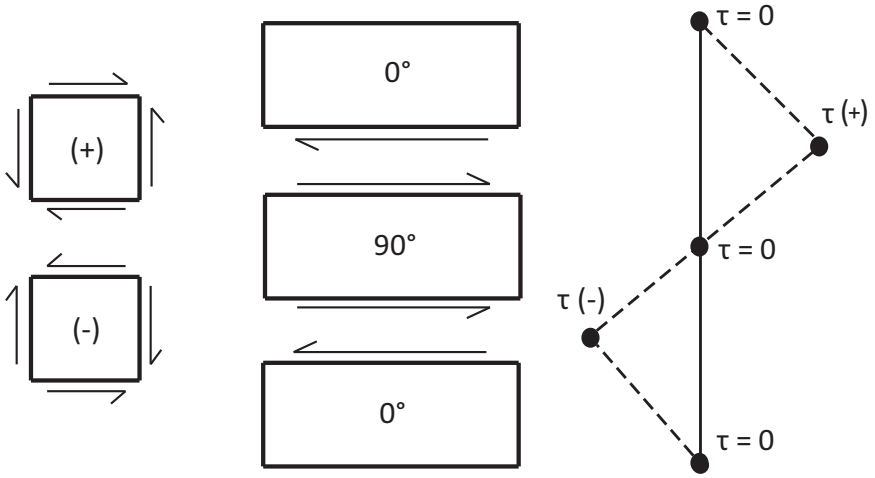

Figure 3: Layerwise linear distribution of intralaminar stress for a $[0/90/0]_S$ laminate.

the cracked and adjacent laminas. Such stress is zero at the top and bottom of the laminate because those are free surfaces. It is also zero at the mid-surface due to symmetry, i.e., all variables must be symmetric with respect to the mid-surface ($\tau_{xz}^{(+)} = \tau_{xz}^{(-)}$), but to satisfy equilibrium, shear stress must have opposite signs on opposite sides of an interface ($\tau_{xz}^{(+)} = -\tau_{xz}^{(-)}$), so the interlaminar stress must be null at the mid-surface.

Furthermore, to satisfy equilibrium inside each lamina, the intralaminar shear stress must have opposite signs on the top and bottom of each lamina. Therefore, its distribution through the thickness must be an odd function. The simplest odd function is a linear distribution, as shown in Figure 3.

A linear distribution of shear stress in a lamina requires through the thickness displacements that are not constant, and for the cracked lamina they must be symmetric with respect to the lamina centerline, thus quadratic. Although better plate kinematics do exist, for example see [40], we have chosen the simplest of them, in order to arrive at an analytical solution. Since the solution of the equations of elasticity for such a problem is intractable, additional approximations are introduced, which reduce the problem to 1D.

Let's introduce the following averaging functions

$$\hat{\phi} = \frac{1}{h_i} \int_{h_i} \phi(z)\, dz \tag{20}$$

$$\hat{\phi}' = \frac{1}{h_i} \int_{z^{i-1,i}}^{z^{i,i+1}} \phi(z^{i-1,i} - z)\, dz \tag{21}$$

Equation (20) provides the average of any function ϕ over the thickness of a lamina. When ϕ is the displacement $u_1^i(x,z)$, equation (20) provides the average displacement $\hat{u}$ of a lamina, as shown in Figure 4. Equation (21) provides the displacement of a lamina relative to the top interface, the later denoted as the $i, i+1$ interface, where i is the lamina number stating with $i = 1$ at the bottom of the laminate.

Let's consider the generic laminate displayed in Figure 5 and the coordinate system shown in Figure 6. The interlaminar stress is assumed to be linear, as follows

$$\tau_{xz}^i(x,z) = \tau_{xz}^{i,i+1}(x) + \left[\tau_{xz}^{i-1,i}(x) - \tau_{xz}^{i,i+1}(x)\right] \frac{z^{i,i+1} - z}{h_i} \tag{22}$$

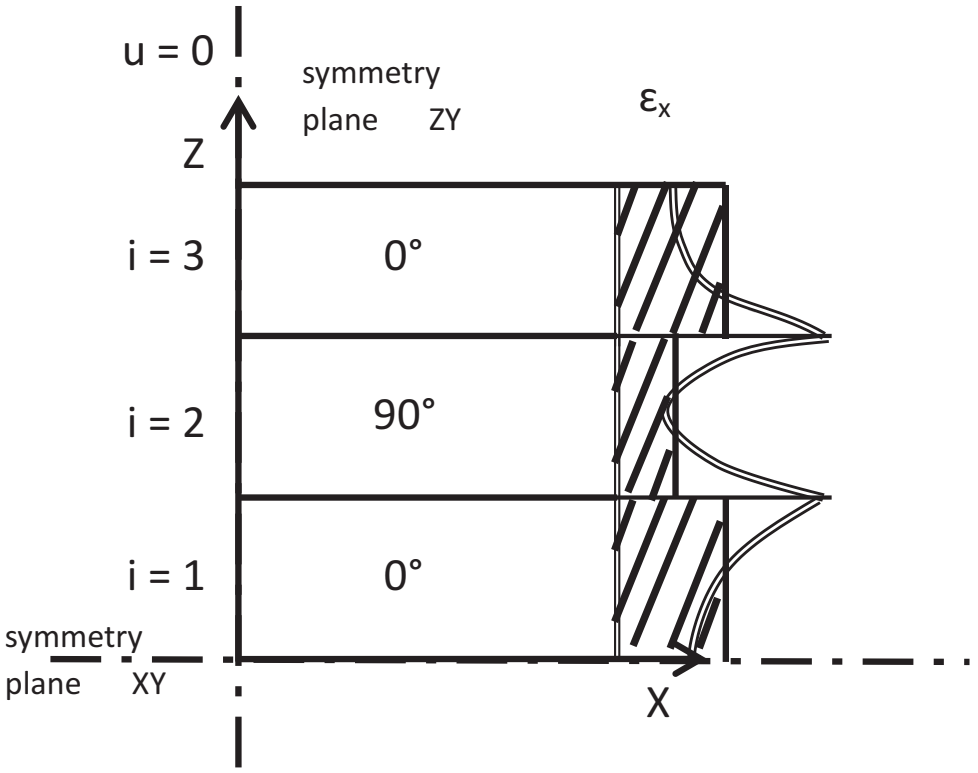

Figure 4: Through-the-thickness distribution of displacement for a $[0/90/0]_S$ laminate: actual and averaged.

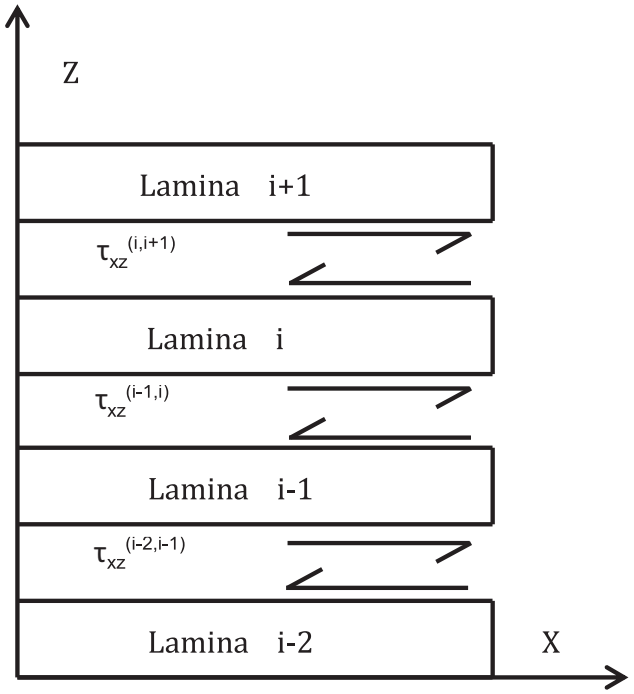

Figure 5: Generic laminate illustrating the numbering of laminas and interface shear stresses.

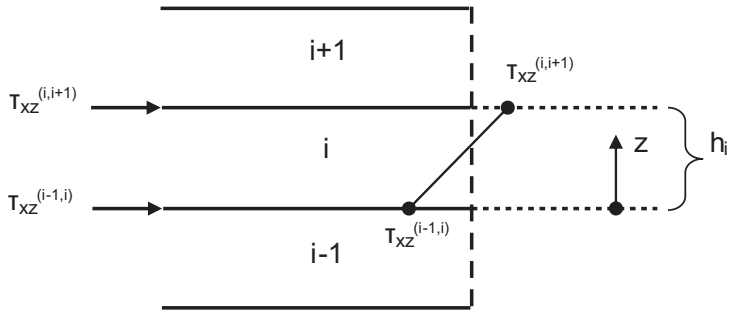

Figure 6: Local coordinate system at lamina i.

Note that assuming intralaminar stress τ_{xz}^i to be linear through the thickness implies a quadratic displacement $u_1^i(x,z)$ distribution through the thickness. Therefore, equation (9) represents the kinematics of the laminate with a piece-wise quadratic deformation that satisfies zero interlaminar stress on the surfaces of the laminate, as depicted in Figure 3. Calculating the weighted average (21) of (12) with τ_{xz}^i given by (22), we get

$$\frac{1}{h_i}\int_{z^{i-1,i}}^{z^{i,i+1}} \frac{\partial u^i}{\partial z}(z^{i,i+1}-z)dz = \frac{1}{h_i}\,\bar{S}_{55}^i \int_{z^{i-1,i}}^{z^{i,i+1}} \tau_{xz}^{i,i+1}\,(z^{i,i+1}-z)\,dz + \frac{1}{h_i}\,\bar{S}_{55}^i \int_{z^{i-1,i}}^{z^{i,i+1}} \left[\tau_{xz}^{i-1,i} - \tau_{xz}^{i,i+1}\right] \frac{(z^{i,i+1}-z)^2}{h_i}\,dz \tag{23}$$

where the subscript i has been dropped from u^i, so there is no need to state the lamina number if the argument z clearly indicates to which lamina we are referring to. Next, developing the LHS of (23) we get

$$\frac{1}{h_i}\left[\int_{z^{i-1,i}}^{z^{i,i+1}} \frac{\partial u^i}{\partial z} z^{i,i+1}dz - \int_{z^{i-1,i}}^{z^{i,i+1}} \frac{\partial u^i}{\partial z} z dz\right] \tag{24}$$

Integrating we get

$$\frac{1}{h_i}\,\left[\,z^{i,i+1}\,u^i(z^{i,i+1}) \;-\; z^{i,i+1}\,u^i(z^{i-1,i}) \;+\; z^{i-1,i}\,u^i(z^{i-1,i}) \;-\; z^{i,i+1}\,u^i(z^{i,i+1})\right] + \frac{1}{h_i}\;\int_{z^{i-1,i}}^{z^{i,i+1}} u^i\,dz \tag{25}$$

and simplifying we have

$$\frac{1}{h_i}\,\left[\,z^{i-1,i} \;-\; z^{i,i+1}\,\right]\,u^i(z^{i-1,i}) \;+\; \widehat{u}(i) \tag{26}$$

where $\widehat{u}(i)$ is the average displacement in lamina-i according to (20). In this way, the problem is reduced from 2D to 1D, where the unknown variables $\widehat{u}(i)$ are only function of x. Therefore, (26) reduces to,

$$\widehat{u}(i) - u(z^{i-1,i}) \tag{27}$$

which we realize is equal to

$$\frac{\partial u^i}{\partial z} \tag{28}$$

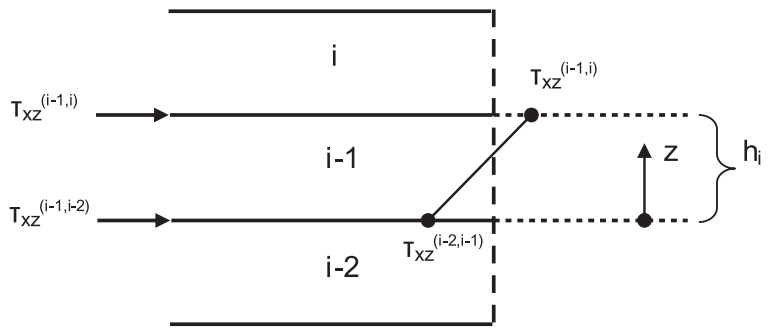

Figure 7: Local coordinate system at lamina *i-1*.

Integrating the first term on the RHS of (23) we have

$$-\frac{\bar{S}_{55}^i}{h_i}\tau_{xz}^{i,i+1}\left[\frac{(z^{i,i+1}-z)^2}{2}\right]_{z^{i-1,i}}^{z^{i,i+1}} = \bar{S}_{55}^i\frac{h_i}{2}\tau_{xz}^{i,i+1} \tag{29}$$

Integrating the second term on the RHS of (23) we have

$$-\frac{\bar{S}_{55}^i}{h_i}\frac{\left[\tau_{xz}^{i-1,i}-\tau_{xz}^{i,i+1}\right]}{h_i}\left[\frac{(z^{i,i+1}-z)^3}{3}\right]_{z^{i-1,i}}^{z^{i,i+1}} = \bar{S}_{55}^i\frac{h_i}{3}\left[\tau_{xz}^{i-1,i}-\tau_{xz}^{i,i+1}\right] \tag{30}$$

Substituting (27),(29),(30) into (23), we get

$$\widehat{u}(i) - u(z^{i-1,i}) = \bar{S}_{55}^i\frac{h_i}{2}\tau_{xz}^{i,i+1} + \bar{S}_{55}^i\frac{h_i}{3}\left[\tau_{xz}^{i-1,i}-\tau_{xz}^{i,i+1}\right] \tag{31}$$

Next, let's consider the coordinate system shown in Figure 7. The interlaminar stress is again assumed to be linear, as follows:

$$\tau_{xz}^{i-1}(x,z) \;=\; \tau_{xz}^{i-2,i-1}(x) \;+\; \left[\tau_{xz}^{i-1,i}(x) - \tau_{xz}^{i-2,i-1}(x)\right]\;\frac{z-z^{i-2,i-1}}{h_{i-1}} \tag{32}$$

Calculating the weighted average (21) of (12) with τ_{xz}^i given by (32), and following the same procedure that led to (31), we get

$$u(z^{i-1,i}) - \widehat{u}(i-1) = \bar{S}_{55}^{i-1}\frac{h_{i-1}}{2}\tau_{xz}^{i-1,i-2} + \bar{S}_{55}^{i-1}\frac{h_{i-1}}{3}\left[\tau_{xz}^{i-1,i}-\tau_{xz}^{i-2,i-1}\right] \tag{33}$$

Adding (31) and (33) we get

$$\widehat{u}(i) - \widehat{u}(i-1) = \tau_{xz}^{i,i+1}\bar{S}_{55}^i\frac{h_i}{6} + \tau_{xz}^{i-1,i}\left[\bar{S}_{55}^i\frac{h_i}{3} + \bar{S}_{55}^{i-1}\frac{h_{i-1}}{3}\right] + \tau_{xz}^{i-2,i-1}\bar{S}_{55}^{i-1}\frac{h_{i-1}}{6} \tag{34}$$

Equation (34) provides the step change in average displacement from one lamina to the next in terms of the intralaminar shear values. But actually what is needed is the inverse, i.e., and equation for the intralaminar shear in terms of displacements. To obtain such relationship, we write (34) for the N-1 interfaces, as follows

$$\begin{Bmatrix} \widehat{u}(2)-\widehat{u}(1) \\ \widehat{u}(3)-\widehat{u}(2) \\ \vdots \\ \widehat{u}(N)-\widehat{u}(N-1) \end{Bmatrix} = [H]\begin{Bmatrix} \tau_{xz}^{1,2} \\ \tau_{xz}^{2,3} \\ \vdots \\ \tau_{xz}^{N-1,N} \end{Bmatrix} \tag{35}$$

where [H] collects the coefficients in (34). Inverting it, we get

$$\tau_{xz}^{i,i+1} = \sum_{j=1}^{N-1} H_{i,j}^{-1} \left[\widehat{u}(j+1) - \widehat{u}(j)\right] \tag{36}$$

Next, calculating the step difference between the intralaminar stresses in terms of the step difference between the average displacements across the N+1 interfaces, including the mid-surface and the bottom surface of the laminate, we get

$$\tau_{xz}^{i,i+1} - \tau_{xz}^{i-1,i} = \sum_{j=1}^{N-1} \left[H_{i,j}^{-1} - H_{i-1,j}^{-1}\right] \left[\widehat{u}(j+1) - \widehat{u}(j)\right] \tag{37}$$

For the first lamina, $i = 1$, $\tau_{xz}^{0,1} = 0$ and $H_{0,j} = 0$ on the bottom surface of the laminate because it is a free surface. For the mid-surface of the laminate, $i = N$, $\tau_{xz}^{N,N+1} = 0$ and $H_{N+1,j} = 0$ due to symmetry.

5 Equilibrium

Based on assumptions (5),(4),(22),(32), the 3D equations of equilibrium reduce to 2D as follows

$$\begin{aligned} \frac{\partial \widehat{\sigma}_x}{\partial x} + \frac{\tau_{xz}^{i,i+1} - \tau_{xz}^{i-1,i}}{h_i} &= 0 \\ \sigma_y &= C(x) \\ \sigma_z &= 0 \end{aligned} \tag{38}$$

where $C = 0$ for plane stress. Substituting (10), (37), and (18) (plane stress) into (38) we get

$$\begin{aligned} &E_x^i \frac{\partial^2 \widehat{u}(i)}{\partial x^2} - \frac{[H_{i-1,1}^{-1} - H_{i,1}^{-1}]}{h_i} \widehat{u}(1) + \frac{[H_{i,1}^{-1} - H_{i-1,1}^{-1} - H_{i,2}^{-1} + H_{i-1,2}^{-1}]}{h_i} \widehat{u}(2) \\ &+ \ldots + \frac{[H_{i,2}^{-1} - H_{i-1,2}^{-1} - H_{i,N-1}^{-1} + H_{i-1,N-1}^{-1}]}{h_i} \widehat{u}(N-1) + \frac{[H_{i,N-1}^{-1} - H_{i-1,N-1}^{-1}]}{h_i} \widehat{u}(N) \end{aligned} \tag{39}$$

Letting $\ddot{u}_i = \partial^2 \widehat{u}(i)/\partial x^2$, (39) can be written as

$$[M]\{\ddot{u}_i\} + [K]\{u_i\} = 0 \tag{40}$$

which can be transformed into

$$\{\ddot{u}_i\} + [D]\{u_i\} = 0 \tag{41}$$

where $[D] = [M]^{-1}[K]$. The matrix [D] can be re-written in terms of its eignevalues [A] and eigenvectors [V] as

$$[D] = [V][A][V]^{-1} \tag{42}$$

Next, applying the change of variable

$$\{\ddot{Z}\} = [V]^{-1}\{\ddot{u}_i\} \tag{43}$$

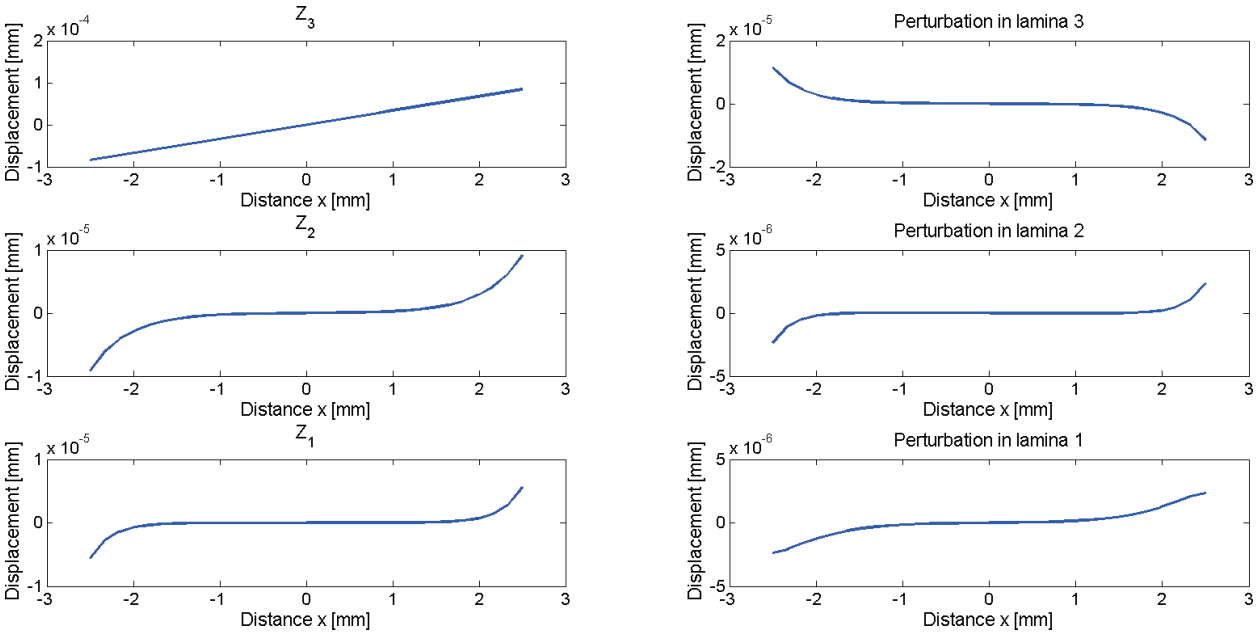

Figure 8: Left: elemental functions. Right: Deformation components. LSS: $[0/\pm 15/90_2]_S$ with $\lambda = 0.2\ [1/mm]$.

we get an uncoupled system of ordinary differential equations (noting that [A] is diagonal)

$$\{\ddot{Z}_i\} + [A]\{Z_i\} = 0 \tag{44}$$

The exact solution to (44) is

$$Z_i = r_i \exp(x\sqrt{-A_i}) + s_i \exp(-x\sqrt{-A_i}) \tag{45}$$

where A_i are the eigenvalues and r_i, s_i, are constants to be found in terms of the boundary conditions. The average displacement in the laminas can be written as a linear combination

$$\widehat{u}_i = \sum_{j=1}^{N} V_{ij} Z_j \tag{46}$$

Taking the origin of the coordinate system at the center of the representative volume element (RVE), as shown in Figure 1, the y-z plane is a plane of symmetry. Therefore, $\widehat{u}_i(x=0) = 0$, then $s_i = -r_i$, and (45) becomes

$$Z_i = r_i \left(\exp(x\sqrt{-A_i}) - \exp(-x\sqrt{-A_i})\right) \tag{47}$$

Since the eigenvalues are all negative, (47) can be written as

$$Z_i = p_i \sinh(x\sqrt{-A_i}); \quad i = 1 \ldots N \tag{48}$$

where $p_i = 2r_i$.

Equation (48) implies that the deformation $\widehat{u}_i$ in (46) is a summation of hyperbolic functions as shown on the left hand side of Figure 8. One of the components (Z_3 in the figure) represents an

homogeneous deformation and the rest are perturbations to correct the solution near the cracks at $\pm\ell$. Let's say this component is Z_s ($s = 3$ in the figure). To describe the homogeneous deformation $u_o(x)$, which is almost linear in the domain $-\ell < x < \ell$, with a *sinh* function, the eigenvalue A_s must be extremely small, so that the *sinh* becomes almost linear in that range. In fact, numerical results confirm that eigenvalue is extremely small for every case analyzed in this work.

A very small eigenvalue results in a very small amplitude for the *sinh*, thus a very large constant p_s is needed to recover the deformation. This pair of very small/very large eigenvalue/constant leads to numerical problems. To avoid such problems, the homogeneous deformation can be approximated by a zero eigenvalue ($A_s = 0$) and a linear function $Z_s = x$. Then, we propose to substitute (49) for (46). That is,

$$\widehat{u}_i = \sum_{j=1}^{N} (1 - \delta_{js}) V_{ij} Z_j + \epsilon_x^0 \, x \tag{49}$$

where ϵ_x^0 is the constant strain corresponding to the homogeneous deformation. In fact, ϵ_x^0 is the mid-surface strain that would be calculated with CLT for the intact laminate, but in this work, ϵ_x^0 is calculated along with the remaining constants to be determined using the boundary conditions in Section 5.1, so that it can be recalculated for any crack density.

5.1 Boundary conditions

5.1.1 Homogeneous deformation on the boundary

The deformation of the boundary of the RVE must be compatible with the rest of the laminate. In this case, this means that the average displacements of all laminas except the cracking one must be the same

$$\widehat{u}_m(\pm\ell) = \widehat{u}_r(\pm\ell); \quad \forall\, m \neq k \tag{50}$$

where lamina r is a lamina that is not cracking, taken as reference. In the computer implementation, $r = 1$ if lamina 1 is not cracking, else $r = 2$.

5.1.2 Stress free crack surface

The cracking lamina k has cracks on the surface of the RVE at $x = -\ell, \ell$, as shown in Figure 1. Crack surfaces are stress free, as follows

$$\int_{-1/2}^{1/2} \widehat{\sigma}_x^k(\ell)\, dy = 0 \tag{51}$$

where the integration limits represent a RVE that has unit length in the y-direction, i.e., in the fiber direction of the cracking lamina. Using (10) and (18) (plane stress), we get

$$E_x^k \int_{-1/2}^{1/2} \left(\frac{\partial \widehat{u}_k(\ell)}{\partial x} - \widehat{\alpha}_x^k \Delta T \right) dy = 0 \tag{52}$$

which simplifies to

$$\dot{\widehat{u}}_k(\ell) = \dot{\widehat{u}}_k(-\ell) = \widehat{\alpha}_x^k \Delta T \tag{53}$$

5.1.3 External load

The applied load N_x, if any, is applied to the boundary of all the laminas except the cracked one because the later has a free surface on the boundary. Therefore, the load equilibrium on the boundary of the RVE excludes the cracked lamina, as follows

$$\sum_{i=1}^{N}(1-\delta_{ik})h_i\int_{-1/2}^{1/2}\widehat{\sigma}_x^i(\ell)\,dy = N_x = h\widehat{\sigma}_x \tag{54}$$

where $h=\sum_{i=1}^{N}h_i$ is the thickness of the symmetric half of the laminate, k is the cracking lamina, δ is the Kronecker symbol, and $\widehat{\sigma}_x$ without a superscript is the average stress applied to the laminate. Using (10) and (18) (plane stress), we get

$$\sum_{i=1}^{N}(1-\delta_{ik})h_iE_x^i\int_{-1/2}^{1/2}\left(\frac{\partial\widehat{u}_i(\ell)}{\partial x}-\widehat{\alpha}_x^i\Delta T\right)dy = h\hat{\sigma}_x \tag{55}$$

which simplifies to

$$\sum_{i=1}^{N}(1-\delta_{ik})h_iE_x^i\dot{\widehat{u}}_i(\ell) = h\hat{\sigma}_x+\sum_{i=1}^{N}(1-\delta_{ik})h_iE_x^i\widehat{\alpha}_x^i\Delta T \tag{56}$$

Note that macroscopically the cracked lamina still supports load that is transferred from the uncracked to the cracked laminas by intralaminar shear in the vicinity of the crack.

6 Reduced Laminate Stiffness

The boundary conditions described in the previous section allows us to determine the constants p_i in (48) for $i\neq s$, that is N-1 values, plus ϵ_x^0 in (49). To do this, one substitutes (49) into the boundary conditions (50), (53), and (56).

Applying $\widehat{\sigma}_x=1,\Delta T=0$, allows us to calculate the degraded modulus of the laminate E_x as a function of crack density λ_k. When a unit stress $\widehat{\sigma}_x=1$ is applied, the resulting laminate deformation $\widehat{\epsilon}_x=\widehat{u}(\ell)/\ell$ is obtained using (20). It follows that the engineering modulus is simply the inverse of S_{11}, as follows

$$E_x = 1/\widehat{\epsilon}_x \quad ; \quad \text{for } \widehat{\sigma}_x=1,\Delta T=0 \tag{57}$$

7 Results and discussion

Two materials have been selected for this section, Fiberity/HyE-9082A [35,36] and Avimid-K/IM6 [23]. Numerical results are compared with experimental data [23, 35, 36] and 3D finite element predictions [31]. The material properties are tabulated in [31].

7.1 Comparison with experimental data and FEA

Comparison with experimental data and finite element results are presented in Figures 9, 10, 11 for two materials and several laminates. The laminate modulus by CLT shown in the figures is the value of ϵ_x^0 (see (49)) calculated for every crack density λ. It can be seen that it remains constant and equal to E_x^0 calculated by CLT for the intact laminate ($\lambda=0$). The difference between this constant value and the reported $E_x(\lambda)$ is physically caused by the cracks and numerically captured by the $N-1$ perturbation terms of the solution in (49).

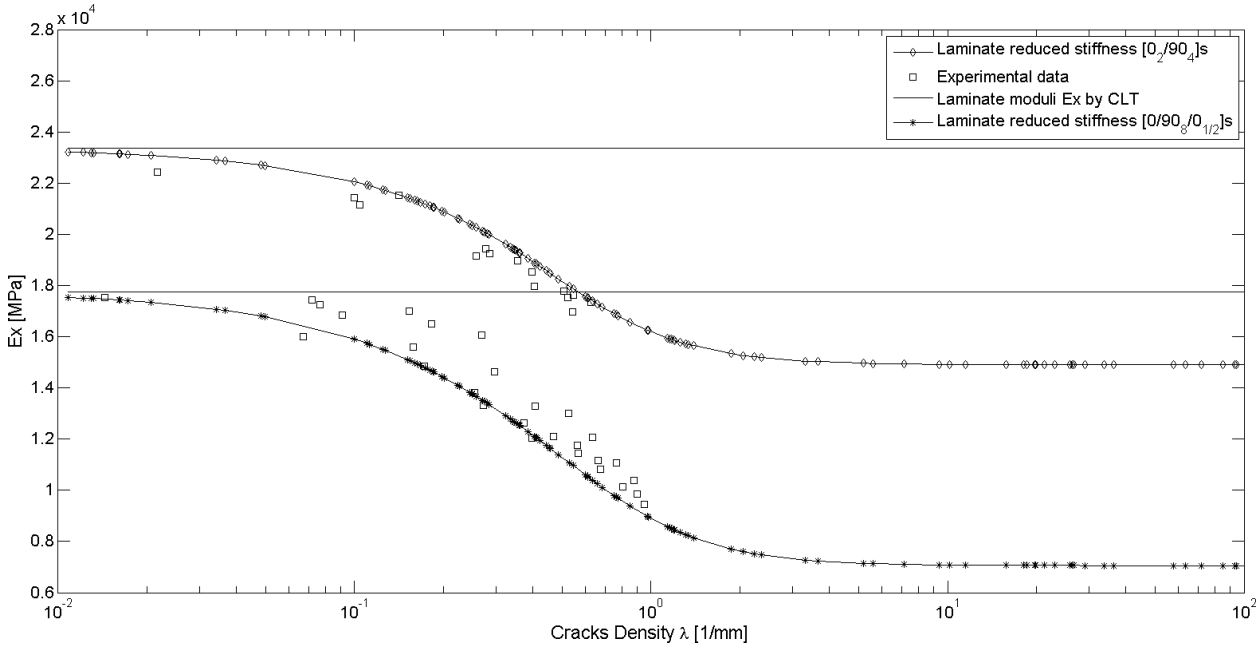

Figure 9: Prediction of laminate modulus vs. crack density for $[0_2/90_4]_S$ and $[0/90_8/0/90_8/0]_T$ Fiberite/HyE-9082A.

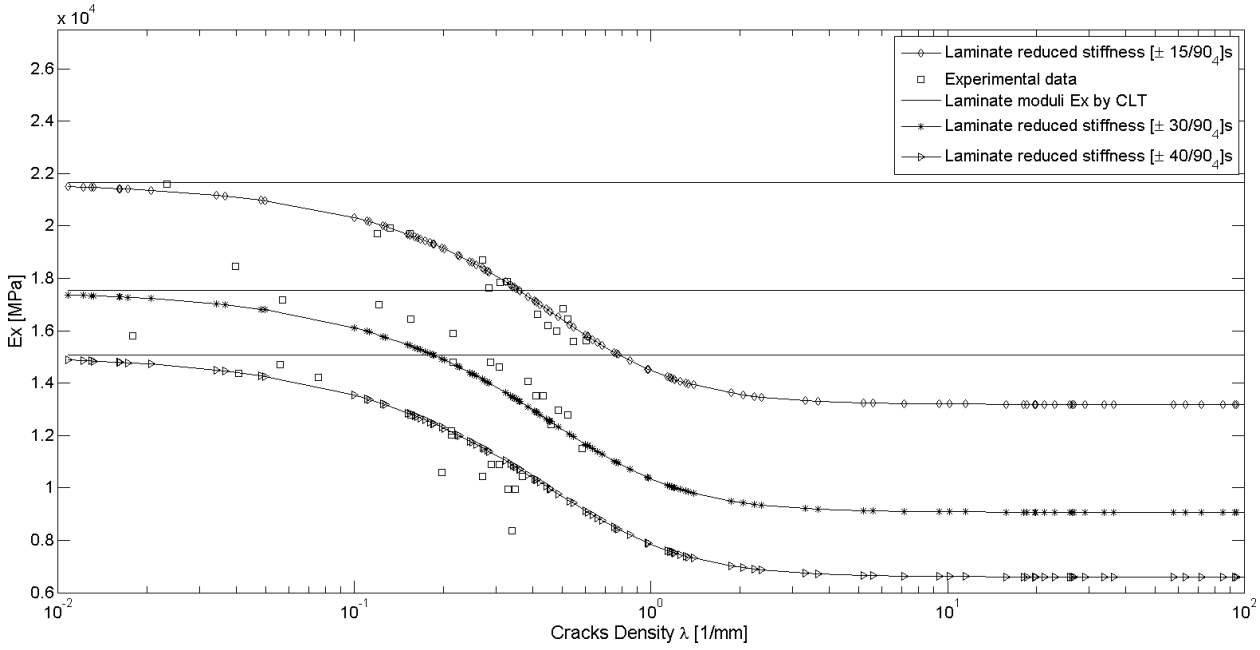

Figure 10: Prediction of laminate modulus vs. crack density for $[\pm\theta/90_4]_S$ Fiberite/HyE-9082A with $\theta = 15, 30, 40$.

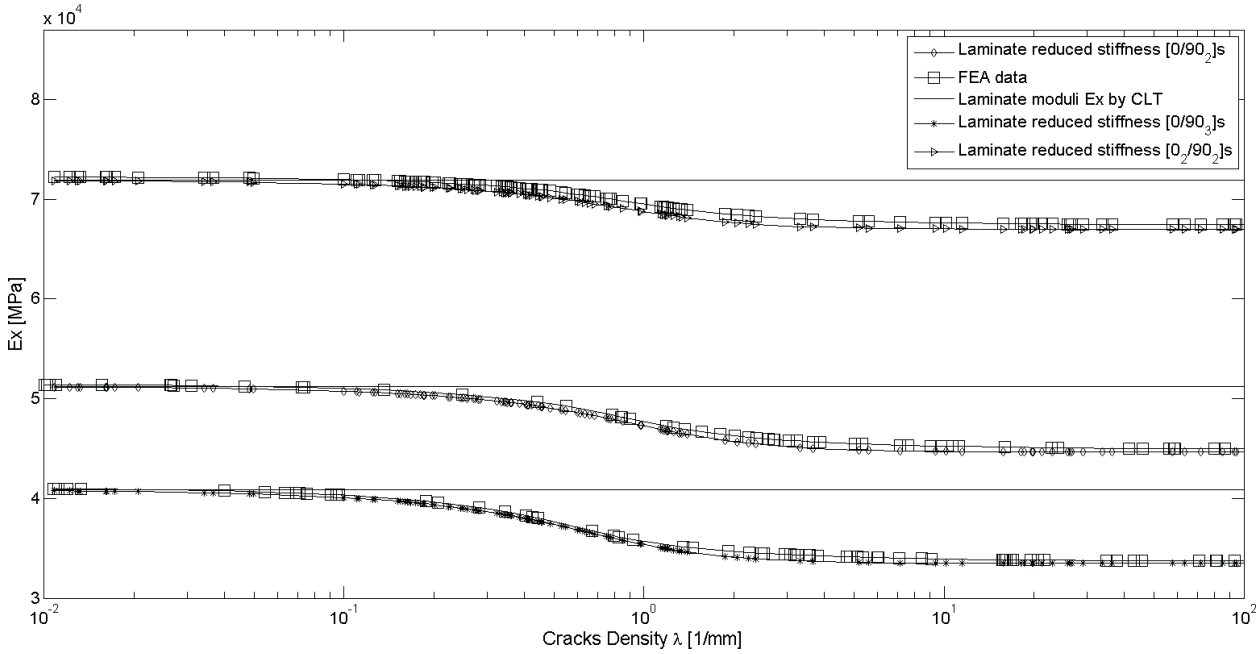

Figure 11: Prediction of laminate modulus vs. crack density for $[0/90_2]_S$, $[0/90_3]_S$, and $[0_2/90_2]_S$ Avimid-K/IM6.

7.2 Intralaminar stress fields

Intralaminar stress are necessary near the crack to transfer the load between the loaded laminas (denoted by subscript m) and the cracked lamina (denoted by subscript k). The intralaminar stress vanishes far away from the crack, once all of the load has been redistributed in the laminate.

Calculated intralaminar stress $\tau_{xz}(x)$ between two cracks located at $x = \pm\ell$ are shown in Figure 12 for the interface 0/90 in a $[0_2/90_4]_S$ laminate and in Figure 13 for the two interfaces in a $[0/\pm 15/90_2]_S$ Fiberite/HyE-9082A. In the legend, the interfaces are denoted by the pair of angles of the adjacent laminas. Recall that $\tau_{xz} = 0$ at the mid-surface due to laminate symmetry.

Calculated intralaminar stress through the thickness $\tau_{xz}(z)$ at the crack surface located at $x = \ell$ is shown in Figure 14 for the $[0_2/90_4]_S$ Fiberite/HyE-9082A laminate. Recall that $\tau_{xz} = 0$ at the mid-surface due to laminate symmetry and at the bottom surface because the later is a free surface.

Note that the approximation can be refined by modeling individual laminas instead of lumping them together into a single, thicker, equivalent lamina. Furthermore, it is possible to refine the model by sub-dividing laminas into a number n of sub-laminas. This cannot be done with the cracking lamina because the crack spans the entire thickness. To show the effect of model refinement, intralaminar stress through the thickness $\tau_{xz}(z)$ at the crack surface located at $x = \ell$ for the $[0_2/90_4]_S$ Fiberite/HyE-9082A laminate are shown in Figure 14 for $n = 1$, Figure 15 for $n = 2$, Figure 16 for $n = 4$, and Figure 17 for $n = 8$, where n is the number of sub-laminas used to subdivide the 0_2 lamina.

It can be seen that the maximum value at the 0/90 interface increases with the number of sub-laminas. This means that the assumption of linear intralaminar stress is not exact. Furthermore, the maximum value of intralaminar stress converges as the number of sub-laminas, in a piece-wise representation on intralaminar stress, increases from 1 to 8. The convergence plot is shown in Figure 18.

Also, it can be seen, particularly in Figure 17, that the intralaminar stress gradient is confined

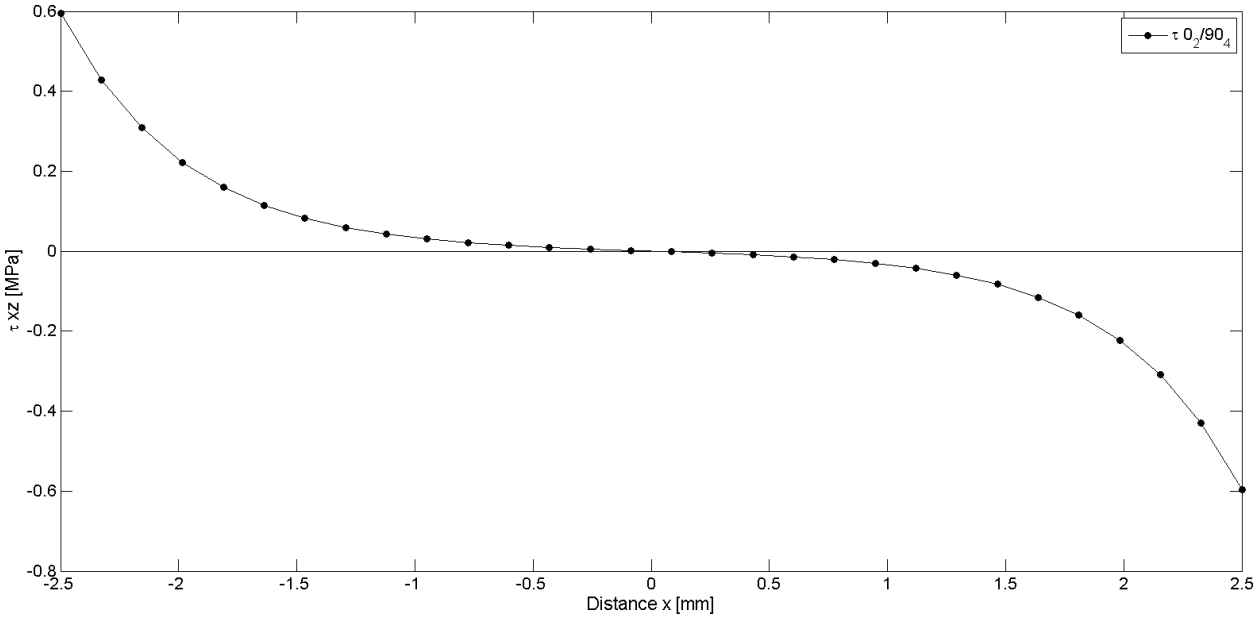

Figure 12: Intralaminar stress $\tau_{xz}(x)$ on the 0/90 interface of a $[0_2/90_4]_S$ Fiberite/HyE-9082A.

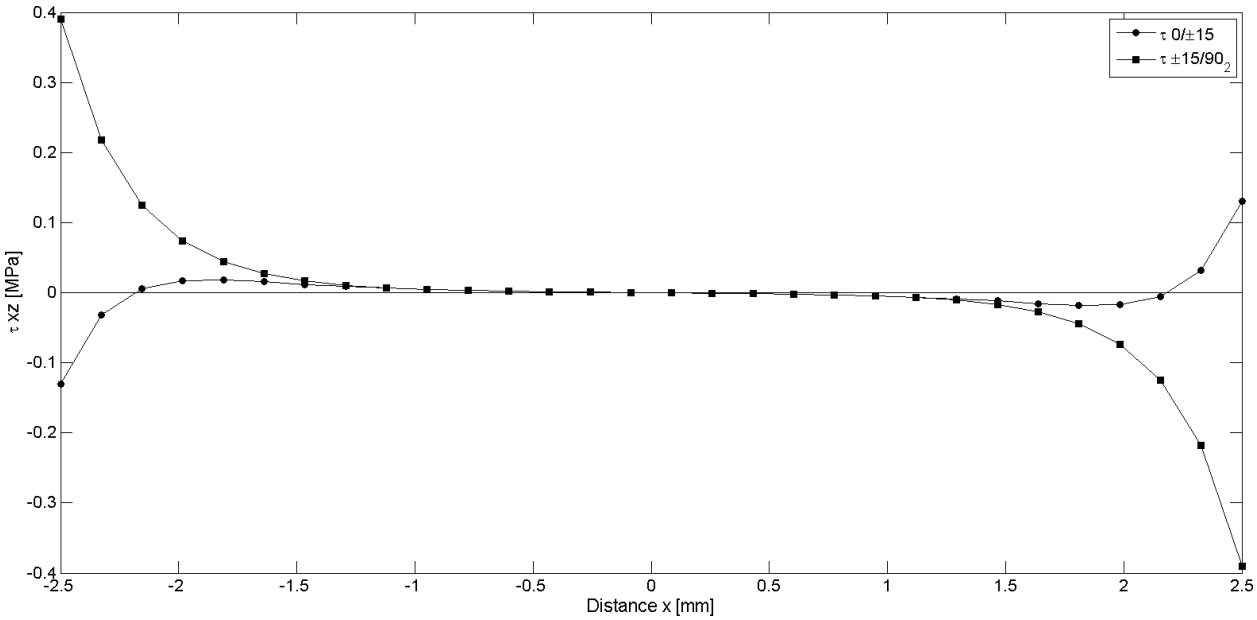

Figure 13: Intralaminar stress $\tau_{xz}(x)$ at the interfaces of a $[0/\pm 15/90_2]_S$ Fiberite/HyE-9082A.

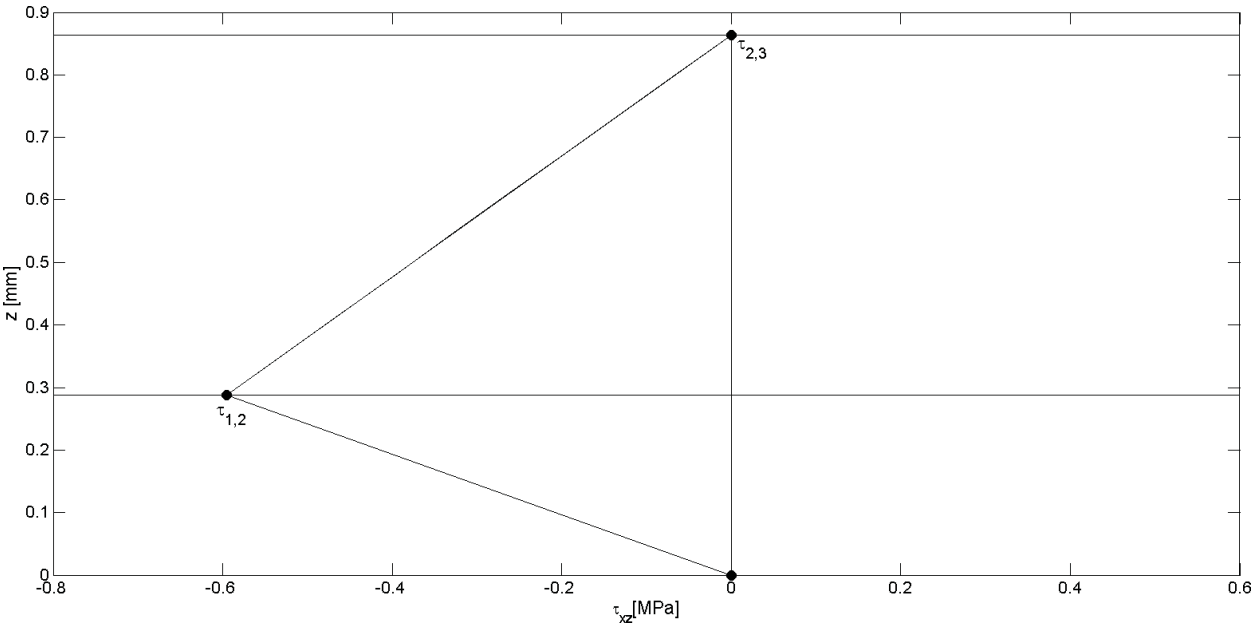

Figure 14: Intralaminar stress $\tau_{xz}(\ell)$ through the thickness of a $[0_2/90_4]_S$ Fiberite/HyE-9082A.

to the vicinity of the 0/90 interface and it vanishes away from it. It is worth noticing that all formulations in the literature use linear distribution of intralaminar stress, not only in the adjacent lamina but over an entire, equivalent sub-laminate that often encompasses all of the intact (non damaging) laminas on either side (top and bottom) of the cracking lamina [16, 22, 28], etc.

7.3 Displacement components

The elementary functions Z_i that result from the exact solution to the problem are shown in Figure 8 (left) for the $[0/\pm 15/90_2]$ laminate. It can be seen that Z_3 is linear, resulting in a homogeneous (linear) *component* of displacement $\hat{u}_i = V_{i3}Z_3$ for all laminas i, with constant strain ϵ_x^0. This is called *fundamental solution*. The remaining components are perturbations that appear in the exact solution to produce the intralaminar stress that redistributes the load between cracked and intact laminas.

The average displacement perturbation in each lamina $\widehat{u}(i) - \epsilon_x^0$ are shown in Figure 8 (right). In the literature, the value of the ineffective length δ (representing the extent of shear lag) is often assumed due to the difficulty in calculating it, but in this case it can be calculated from the exact solution for the perturbations. The ineffective length is defined [41] as the distance δ for which the perturbations decrease to 10% of their maximum value [42, 43]. In this way, δ is calculated for Figure 12 and 13 and the results are shown in the Table 1.

Laminate	*Interface*	δ [mm]
$[0/\pm 15/90_2]$s	$0/\pm 15$	0.975
	$\pm 15/90_2$	0.74
$[0_2/90_4]s$	$0_2/90_4$	1.207

Table 1: Calculated ineffective length δ.

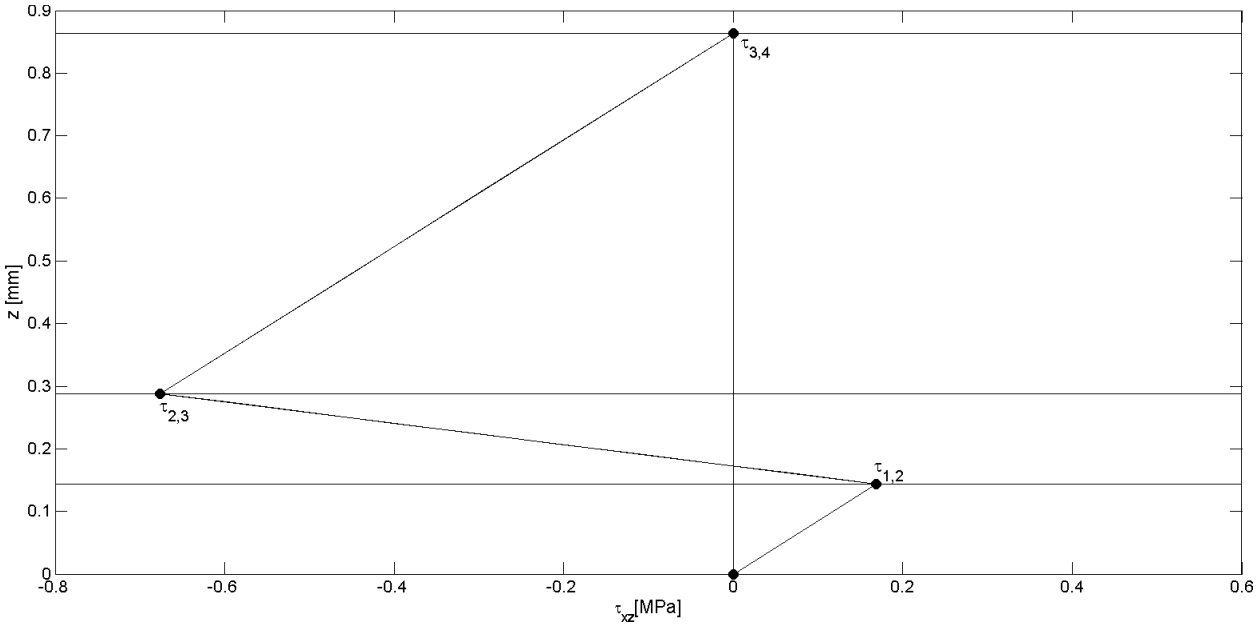

Figure 15: Intralaminar stress $\tau_{xz}(\ell)$ through the thickness of a $[0_2/90_4]_S$ with the 0° lamina divided in *two* sub-laminas.

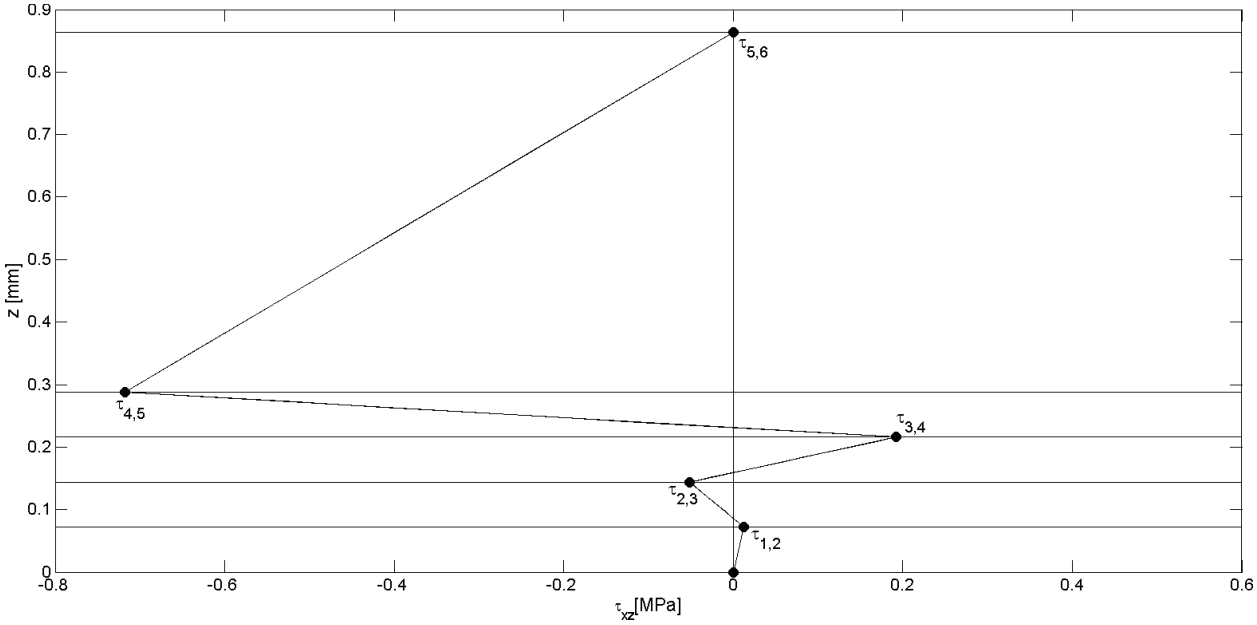

Figure 16: Intralaminar stress $\tau_{xz}(\ell)$ through the thickness of a $[0_2/90_4]_S$ with the 0° lamina divided in *four* sub-laminas.

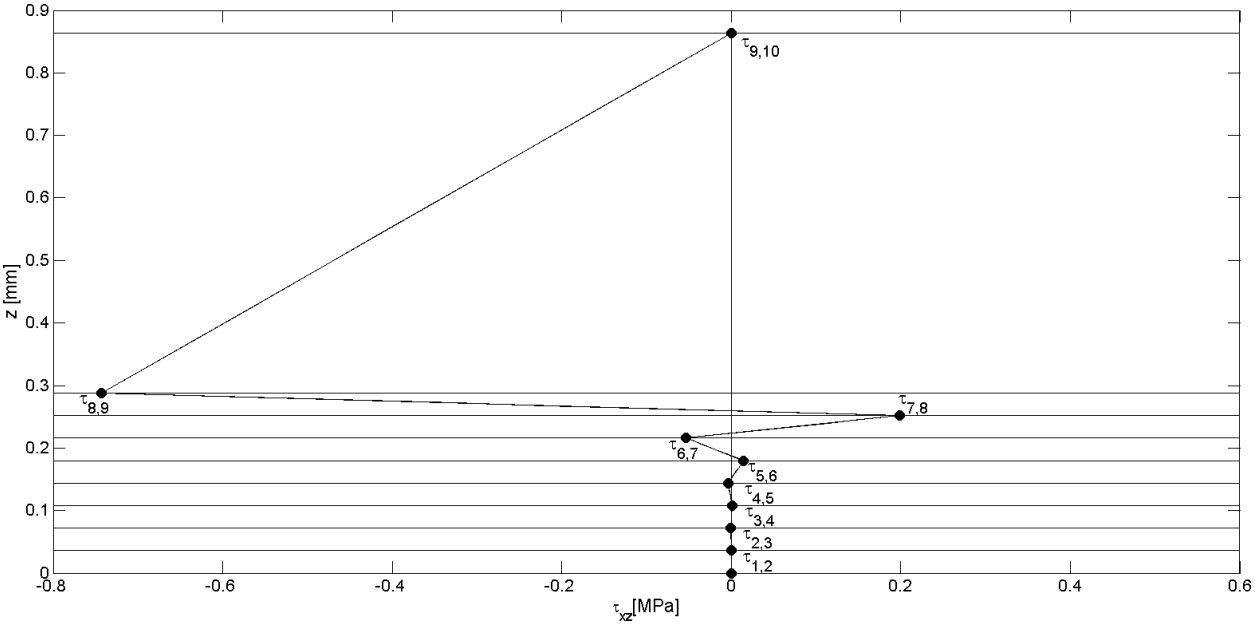

Figure 17: Intralaminar stress $\tau_{xz}(\ell)$ through the thickness of a $[0_2/90_4]_S$ with the 0° lamina divided in *eight* sub-laminas.

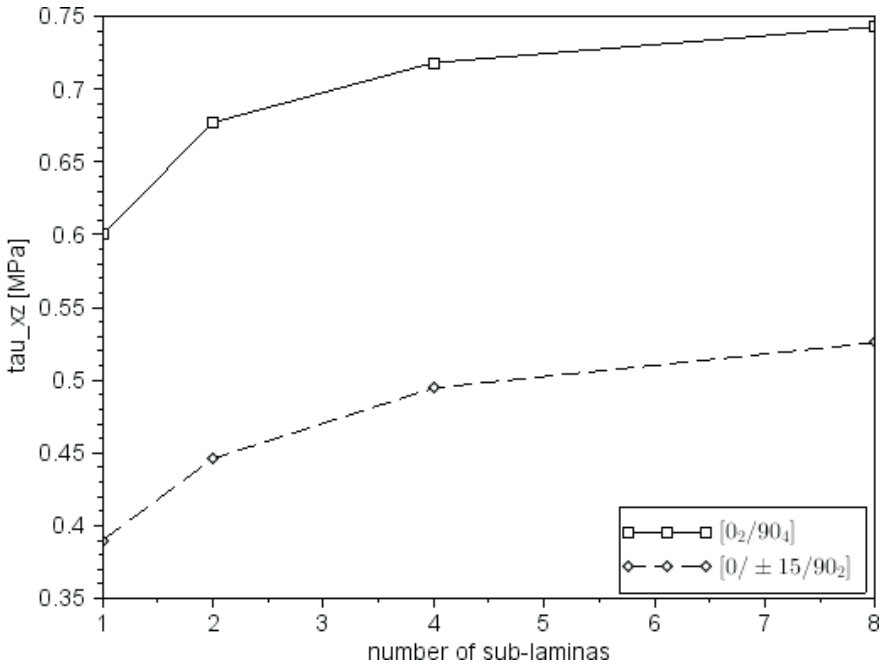

Figure 18: Maximum intralaminar stress $\tau_{xz}(\ell)$ as a function of the number of sub-laminas in the 0 and ±15 laminas.

7.4 Condition number

The condition number for an eigenvalues problem is defined as division between the maximum and minimum eigenvalue. Ordering the eigenvalues by descending value, the condition number for the problem (46) is $C_n = A_1/A_n \gg 1$ whose values are unfavorable for numerical computation. On the other hand, the condition number for (49) is $C_{n-1} = A_1/A_{n-1} \sim 10^1$. Therefore, using (49) instead of (46) allows us to solve the same problem but with condition number $C_{n-1} \simeq O(1)$. A comparison between the condition number of the original eignevalue problem (46) and the new one (49) is shown in Table 2.

Material	*Laminate*	C_n	C_{n-1}	A_1	A_{n-1}	A_n
C	$[0/90_2]s$	$3.961e+16$	19.922	-10.655	-0.535	-2.690e-16
C	$[0/90_3]s$	$3.546e+16$	14.837	-5.454	-0.368	-1.538e-16
C	$[0_2/90_2]s$	$7.398e+16$	33.096	-8.117	-0.245	-1.097e-16
G	$[0_2/90_4]s$	$2.584e+16$	6.736	-3.622	-0.537	-1.401e-16
G	$[0/\pm 15/90_2]s$	$3.648e+15$	3.216	-17.059	-5.303	-4.675e-15
G	$[\pm 15/90_4]s$	$9.118e+15$	4	-20.891	-5.223	-2.231e-15
G	$[\pm 30/90_4]s$	$8.729e+16$	4	-29.105	-7.276	-3.334e-16
G	$[\pm 40/90_4]s$	$9.436e+15$	4	-38.471	-9.618	-4.077e-15
G	$[0/90_8/0_{1/2}]s$	$4.092e+18$	4.960	–7.792	-1.571	-1.904e-18

C: IM6(Carbon)/Avimid-K G: Fiberite(Glass)/HyE-9082A

Table 2: Condition number C and eigenvalues A.

8 Conclusions

The exact solution allows us to identify the source of ill-conditioning that occurs when the solution is formulated in terms of displacements, as it has been done so far in the literature. In that case, a very small eigenvalue is necessary to have one *sinh* function that is almost-linear, and that function is in turn needed to represent the overall stretching of the laminate, i.e., the CLT deformation without cracks. The tiny eigenvalue, and its conjugate huge eigenvector, lead to numerical problems. The remaining eigenvalues/eigenvectors, all with order of magnitude $O(1)$, represent displacement perturbations near the crack that are needed to obtain interlaminar shear stress involved in shear lag transfer of load from uncracked to cracked laminas. The proposed solution (49) eliminates the numerical problem. Furthermore, the proposed exact solution for the perturbations allows for the computation of the interlaminar shear stress at all interfaces and along the entire length between cracks. As a corollary, it allows for computation of the ineffective length (shear lag). Furthermore, the proposed formulation allows for subdividing intact laminas into sub-laminas to increase the accuracy of the interlaminar stress computation, which is shown to converge as the number of sub-laminas increases. It also reveals that assuming a linear distribution of interlaminar stress is indeed an approximation, whose effect on the solution can be now assessed using the proposed formulation. In addition, the exact solution provides a benchmark for approximate and numerical solutions.

References

[1] R. Talreja and C.V. Singh. *Damage and Failure of Composite Materials*. Cambridge University Press, 2012.

[2] C. G. Davila. Modeling fracture and complex crack networks in laminated composites. In V. Mantic, editor, *Mathematical Methods and Models in Composites*, Computational and Experimental Methods in Structures. Imperial College Press, 2013.

[3] G. J. Dvorak, N. Laws, and M. Hejazi. Analysis of progressive matrix cracking in composite laminates i. thermoelastic properties of a ply with cracks. *Journal of Composite Materials*, 19(3):216–234, 1985.

[4] E J Barbero and J N Reddy. Modeling of delamination in composite laminates using a layer-wise plate theory. *International Journal of Solids and Structures*, 28(3):373–388, 1991.

[5] M. M. Moure, S. Sanchez-Saez, E. Barbero, and E. J. Barbero. Analysis of damage localization in composite laminates using a discrete damage model. *Composites Part B*, 66:224–232, 2014.

[6] P. Lonetti, R. Zinno, F. Greco, and E. J. Barbero. Interlaminar damage model for polymer matrix composites. *Journal of Composite Materials*, 37(16):1485–1504, 2003.

[7] E. J. Barbero, F. Greco, and P. Lonetti. Continuum damage-healing mechanics with application to self-healing composites. *International Journal of Damage Mechanics*, 14(1):51–81, 2005.

[8] L. N. McCartney. Energy-based prediction of progressive ply cracking and strength of general symmetric laminates using an homogenisation. *Method, Composites Part A*, 36:119–128, 2005.

[9] L. N. McCartney. Energy-based prediction of failure in general symmetric laminates. *Engineering Fracture Mechanics*, 72:909930, 2005.

[10] E. J. Barbero and L. DeVivo. Constitutive model for elastic damage in fiber-reinforced pmc laminae. *International Journal of Damage Mechanics*, 10(1):73–93, 2001.

[11] P. P. Camanho and C. G. Davila. Mixed-mode decohesion finite elements for the simulation of delamination in composite materials. *NASA/TM-2002-211737*, pages 1–37, 2002.

[12] Simulia. *Abaqus Theory Manual, Version 6.10*.

[13] Francesco Freddi and Elio Sacco. An interface damage model accounting for in-plane effects. *International Journal of Solids and Structures*, 51(2526):4230 – 4244, 2014.

[14] P. Maimí, P., P.P. Camanho, J.A. Mayugo, and A. Turon. Matrix cracking and delamination in laminated composites. part ii: Evolution of crack density and delamination. *Mechanics of Materials*, 43(4):194–211, 2011. cited By 2.

[15] P. Maimí, P.P. Camanho, J.A. Mayugo, and A. Turon. Matrix cracking and delamination in laminated composites. part i: Ply constitutive law, first ply failure and onset of delamination. *Mechanics of Materials*, 43(4):169–185, 2011. cited By 15.

[16] S. C. Tan and R. J. Nuismer. A theory for progressive matrix cracking in composite laminates. *Journal of Composite Materials*, 23:1029–1047, 1989.

[17] T. Yokozeki and T. Aoki. Stress analysis of symmetric laminates with obliquely-crossed matrix cracks. *Advanced Composite Materials*, 13(2):121–40, 2004.

[18] P. Ladevèze, O. Allix, J.F. Deü, and D. Lévêque. A mesomodel for localisation and damage computation in laminates. *Computer Methods in Applied Mechanics and Engineering*, 183(1-2):105–122, 2000.

[19] F. Rastellini, S. Oller, O. Salomón, and E. O nate. Composite materials non-linear modelling for long fibre-reinforced laminates: Continuum basis, computational aspects and validations. *Computers and Structures*, 86(9):879–896, 2008.

[20] X. Martinez, F. Rastellini, S. Oller, F. Flores, and E. O nate. Computationally optimized formulation for the simulation of composite materials and delamination failures. *Composites Part B: Engineering*, 42(2):134–144, 2011.

[21] E. J. Barbero, F. A. Cosso, R. Roman, and T. L. Weadon. Determination of material parameters for Abaqus progressive damage analysis of E-Glass Epoxy laminates. *Composites Part B:Engineering*, 46:211–220, 2013.

[22] R. J. Nuismer and S. C. Tan. Constitutive relations of a cracked composite lamina. *Journal of Composite Materials*, 22:306–321, 1988.

[23] S. Liu and J. A. Nairn. Formation and propagation of matrix microcracks in cross-ply laminates. *J Reinf Plas Compos*, pages 158–178, 1992.

[24] E. Adolfsson and P. Gudmundson. Matrix crack initiation and progression in composite laminates subjected to bending and extension. *Int. J. of Solids and Structures*, 36:3131–3169, 1999.

[25] J. Nairn. Matrix microcracking in composites. In R Talreja and J A E Manson, editors, *Polymer Matrix Composites*, volume 2 of *Comprehensive Composite Materials*, pages 403–432. Elsevier, Amsterdam, 2000.

[26] J. Nairn and S. Hu. Matrix microcracking. In R. Talreja, editor, *Damage Mechanics of Composites Materials*, pages 187–243. Elsevier, 2004.

[27] G N Praveen and J N Reddy. Transverse matrix cracks in cross-ply laminates: Stress transfer, stiffness reduction and crack opening profiles. *Acta Mechanica*, 130:3–4, 1998.

[28] J. A. Mayugo, P. P. Camanho, P. Maimi, and C. G. Davila. Analytical modelling of transverse matrix cracking [+-theta/90n]s of composite laminates under multiaxial loading. *Mechanics of Advanced Materials and Structures*, 17(4):237–245, 2010.

[29] D. H. Cortes and E. J. Barbero. Stiffness reduction and fracture evolution of oblique matrix cracks in composite laminates. *Annals of Solid and Structural Mechanics*, 1(1):29–40, 2010.

[30] E. J. Barbero and D. H. Cortes. A mechanistic model for transverse damage initiation, evolution, and stiffness reduction in laminated composites. *Composites Part B*, 41:124–132, 2010.

[31] E. J. Barbero and F. A. Cosso. Benchmark solution for degradation of elastic properties due to transverse matrix cracking in laminated composites. *Composite Structures*, 98:242–252, 2013.

[32] E. J. Barbero, F. A. Cosso, and X. Martinez. Identification of fracture toughness for discrete damage mechanics analysis of glass-epoxy laminates. *Applied Composite Materials*, November:1–18, 2013.

[33] E. J. Barbero and F. A. Cosso. Determination of material parameters for discrete damage mechanics analysis of carbon-epoxy laminates. *Composites Part B*, 56:638–646, 2014.

[34] C.T. Sun. *Mechanics of Aircraft Structures*. Wiley, 1998.

[35] J. Varna, R. Joffe, N. Akshantala, and R. Talreja. Damage in composite laminates with off-axis plies. *Composites Science and Technology*, 59:2139–2147, 1999.

[36] J. Varna, R. Joffe, and R. Talreja. A synergistic damage mechanics analysis of transverse cracking in $[\pm\theta/90_4]_s$ laminates. *Composites Science and Technology*, 61:657–665, 2001.

[37] T. Yokozeki, T. Aoki, and T. Ishikawa. Consecutive matrix cracking in contiguous plies of composite laminates. *International Journal of Solids and Structures*, 42(9-10):2785–2802, 05 2005.

[38] E. J. Barbero. *Introduction to Composite Materials Design*. CRC Press, Philadelphia, PA, second edition, 2011.

[39] A. M. Abad Blazquez, M. Herraez Matesanz, C. Navarro Ugena, , and E. J. Barbero. Acoustic emission characterization of intralaminar damage in composite laminates. In *MATCOMP XIII*, pages 33–38, 2013.

[40] Ferdinando Auricchio, Giuseppe Balduzzi, Mohammad Javad Khoshgoftar, Gholamhosein Rahimi, and Elio Sacco. Enhanced modeling approach for multilayer anisotropic plates based on dimension reduction method and hellingerreissner principle. *Composite Structures*, 118(0):622 – 633, 2014.

[41] B. W. Rosen. Tensile failure of fibrous composites. *AIAA Journal*, 2(11):1985–1991, November 1964.

[42] E. J. Barbero and K. W. Kelly. Predicting high temperature ultimate strength of continuous fiber metal matrix composites. *Journal of Composite Materials*, 27(12):1214–1235, 1993.

[43] K. W. Kelly and E. J. Barbero. Effect of fiber damage on the longitudinal creep of a cfmmc. *International Journal of Solids and Structures*, 30(24):3417–3429, 1993.